Variation of the Air Mass Exposure to Chlorophyll Over Eastern China Seas: an Insight into Marine Biogenic Aerosols

Shengqian Zhou[1], Ying Chen[1], Fanghui Wang[1], Yang Bao[2], Zongjun Xu[1], and Xiping Ding[3]

[1]Fudan University
[2]Shanghai Key Laboratory of Atmospheric Particle Pollution Prevention, Department of Environmental Science & Engineering, Fudan University Jiangwan Campus
[3]Pudong New District Environmental Monitoring Station

November 23, 2022

Abstract

Marine biological activities make substantial influences on aerosol composition and properties. The eastern China seas are highly productive with significant emissions of biogenic substances. Air mass exposure to chlorophyll a (AEC) can be used to indicate the influence of biogenic source on the atmosphere to a certain degree. In this study, the 12-year (2009–2020) daily AEC were calculated over the eastern China seas showing the spatial and seasonal patterns of marine biogenic influence intensity are co-controlled by surface phytoplankton biomass and boundary layer height. The AEC was linearly correlated with aerosol methanesulfonate (MSA) in each of three sub-regions, and the constructed parameterization scheme was applied to simulate the spatiotemporal variation of marine biogenic MSA. This AEC-based approach with observation constraints provides a new insight into the distribution of marine biogenic aerosols which may become increasingly important with the decline of terrestrial input to the studied region.

Variation of the Air Mass Exposure to Chlorophyll Over Eastern China Seas: an Insight into Marine Biogenic Aerosols

Shengqian Zhou[1], Ying Chen[1,2*], Fanghui Wang[1], Yang Bao[1], Xiping Ding[3]，Zongjun Xu[1]

[1]Shanghai Key Laboratory of Atmospheric Particle Pollution Prevention, Department of Environmental Science & Engineering, Institute of Atmospheric Sciences, Fudan University, Shanghai 200438, China.

[2]Institute of Eco-Chongming (IEC), Shanghai 202162, China.

[3]Pudong New District Environmental Monitoring Station, Shanghai 200135, China.

Corresponding author: Ying Chen (yingchen@fudan.edu.cn)

Key Points:

- Air mass exposure to chlorophyll (AEC) is a good indicator for the influence extent of marine biogenic emission on atmospheric environment

- Variation of AEC over the eastern Chin seas is co-controlled by surface chlorophyll *a* and boundary layer height

- AEC-based parameterization provides a new insight into simulating the distribution of marine biogenic aerosols

Abstract

Marine biological activities make substantial influences on aerosol composition and properties. The eastern China seas are highly productive with significant emissions of biogenic substances. Air mass exposure to chlorophyll *a* (AEC) can be used to indicate the influence of biogenic source on the atmosphere to a certain degree. In this study, the 12-year (2009–2020) daily AEC were calculated over the eastern China seas showing the spatial and seasonal patterns of marine biogenic influence intensity are co-controlled by surface phytoplankton biomass and boundary layer height. The AEC was linearly correlated with aerosol methanesulfonate (MSA) in each of three sub-regions, and the constructed parameterization scheme was applied to simulate the spatiotemporal variation of marine biogenic MSA. This AEC-based approach with observation constraints provides a new insight into the distribution of marine biogenic aerosols which may become increasingly important with the decline of terrestrial input to the studied region.

Plain Language Summary

Marine organisms can generate trace gases contributing to the formation and growth of atmospheric aerosols and thereby affect the climate. Along with the great reduction of air pollutants in China and weakening of East Asian winter monsoon, atmospheric transport of substances from mainland to the eastern China seas has declined significantly over the past decade. Accordingly, marine biogenic aerosols become increasingly important, which have not yet been well investigated. In this study, the air mass exposure to chlorophyll *a* (AEC) index representing the influence of marine biogenic source on the air was calculated over the eastern China seas during 2009 to 2020 based on air mass backward trajectories and surface chlorophyll retrieved from satellite images. The AEC values declined from the northwest to southeast region and were especially prosperous in spring, which was associated with the variations of surface chlorophyll *a* and boundary layer height. Taking aerosol methanesulfonate (MSA, a typically biogenic component) as a representative, we showed the capability of using the AEC and observations to simulate the variation of marine biogenic aerosol components. This method enables further exploration of the interaction between natural and anthropogenic aerosols and their environmental and climatic effects.

1 Introduction

Atmospheric aerosols, originating from numerous natural and anthropogenic sources, play critical roles in the Earth's climate system (Pöschl, 2005). Marine biological activities can produce and release a large quantity of organic compounds, which will make great contribution to marine aerosols via primary emissions in the form of sea spray aerosols and secondary formation of sea-to-air transferred gases (Carpenter et al., 2012; O'dowd et al., 2004). It has been estimated that the global emission of marine organic carbon (OC) aerosol was around 8 Tg year^{-1}, comparable to the magnitude of anthropogenic fossil and biofuel OC (Spracklen et al., 2008). The impact of marine biogenic source on aerosols often closely connects to the surface phytoplankton biomass (Mansour et al., 2020b; Rinaldi et al., 2013). For example, marine organic matters dominate the fine-mode aerosol mass during the blooming period and inorganic species are more important with the low-biological activities in the North Atlantic (O'dowd et al., 2004).

The eastern China seas (Bohai, Yellow and East China seas) are adjacent to densely populated eastern China, and the continental outflow of atmospheric pollutants may have notable

63　influence on aerosols over this region (Wang et al., 2016; Xu et al., 2021). Meanwhile, they are
64　highly productive as a result of exogenous input of abundant nutrients, and the emissions of
65　biogenic substances are much larger than oligotrophic seas (Zhang et al., 2014; Zhou et al.,
66　2021). Several cruise and island based observations have shown the significance of marine
67　biogenic source to carbonaceous aerosols (Kunwar and Kawamura, 2014; Li et al., 2022) and
68　specific components (e.g. amines, carboxylic acids, sulfur-containing species) (Guo et al., 2016;
69　Hu et al., 2015; Yang et al., 2009; Zhou et al., 2019). However, the spatiotemporal dynamics of
70　marine biological influence on atmospheric environment and subsequent distributions of
71　biogenic aerosol components are still poorly understood, due partly to the scarcity of field
72　observation.

73　　　Air mass exposure to chlorophyll *a* (AEC), i.e. the weighted average concentration of sea
74　surface chlorophyll *a* (Chl *a*) along the transport path of air mass, is a good surrogate for the
75　extent to which the air mass at a specific site is affected by marine biogenic emissions (Arnold et
76　al., 2010; Blazina et al., 2017; Park et al., 2018). This index encompasses (1) biogenic emission
77　intensity proxied by surface Chl *a* concentration, (2) transport path characterized by air mass
78　backward trajectory, and (3) diffusion and loss indicated by a weighting factor related to
79　transport time. Zhou et al. (2021) have made improvement by adding a term reciprocal to
80　boundary layer height (BLH), since BLH is a critical factor controlling ventilation and thereby
81　concentrations of atmospheric components in the boundary layer. Based on this modified AEC
82　index, the linkage between marine biogenic aerosol and phytoplankton biomass can be examined
83　(Zhou et al., 2021). Aerosol methanesulfonate (MSA), as an important oxidation product of
84　oceanic organism-derived dimethyl sulfide (DMS), is traditionally considered an indicator for
85　marine biogenic sources (Park et al., 2017; Savoie et al., 2002; Yang et al., 2009). It is also one
86　of the most abundant components of secondary organic aerosol (SOA) in marine environment
87　(Facchini et al., 2008). Good correlations have been found between MSA and AEC in coastal
88　seas when removing terrestrial perturbation and constraining air transport within marine
89　boundary layer (MBL, (Zhou et al., 2021)).

90　　　In this study, based on air mass backward trajectories and satellite remote sensing
91　products, we elucidated the spatiotemporal distribution of AEC over the eastern China seas
92　during 2009 to 2020. These results showed how the influence extent of marine biogenic emission
93　on MBL aerosols varies on a regional scale, which has not been addressed before. By integrating
94　historical aerosol observations and AEC values, a parameterization scheme for the concentration
95　of marine biogenic MSA is developed. The results demonstrate the prospect of estimating
96　distribution of marine biogenic aerosols through an observation constrained method on the basis
97　of AEC index. In the end, the potential rising importance of marine biogenic emissions compared
98　to terrestrial transport was discussed by analyzing the decadal trend of terrestrial transport
99　intensity.

100　**2 Materials and Methods**

101　　　2.1 Calculation of Trajectories and Relevant Indexes

102　　　The air mass backward trajectories were calculated by Hybrid Single-Particle Lagrangian
103　Integrated Trajectories (HYSPLIT) model with input of Global Data Assimilation System
104　(GDAS) Archived (1° × 1°) meteorology dataset. The starting height was 100 m and the

105 trajectory duration was 72 h. The BLH at each trajectory endpoint was extracted from GDAS
106 dataset.

107   The AEC value for a specific trajectory was calculated by Equation 1:

108 $$AEC = \frac{\sum_{i=1}^{N_{total}} Chla_i \cdot e^{-\frac{t_i}{72}} \cdot \frac{600}{BLH_i}}{n} \qquad (1)$$

109 where N_{total} is the total number of hourly endpoints (73 containing the receptor point) along
110 the trajectory. $Chla_i$ represents the mean Chl *a* concentration (Terra-MODIS 8-day composite
111 of Chl *a* concentration, $0.042° \times 0.042°$) within a radius of 20 km centered in the *i*th endpoint of
112 a trajectory. t_i and BLH_i are the tracking time (hour) and BLH (m) of the *i*th endpoint,
113 respectively. $e^{-\frac{t_i}{72}}$ is the weighting factor related to tracking time, because the location
114 corresponding to longer transport time has weaker influence on the receptor site due to the
115 diffusion and deposition along the transport. *n* is the number of endpoints with valid Chl *a*
116 concentrations. The detailed calculation processes and associated data filtration rules refer to
117 Zhou et al. (2021).

118   The air mass retention ratio over land (R_L), i.e. the weighted ratio of air transport time
119 over land to the whole duration, was calculated by Equation 2 indicating the influence of
120 terrestrial transport on the receptor site:

121 $$R_L = \frac{\sum_{i=1}^{N_{land}} e^{-\frac{t_i}{72}}}{\sum_{i=1}^{N_{total}} e^{-\frac{t_i}{72}}} \qquad (2)$$

122 where N_{land} is the total number of trajectory endpoints located over land.

123   Based on aerosol observations during four cruises over the eastern China seas (Section
124 2.3 and Text S1), R_L index showed positive relationships with both typical anthropogenic metal
125 Cd and dust-associated metal Al (Figure S1). The average concentrations of Cd and Al for $R_L >$
126 0.75 were 5.8 and 14.5 times higher than for $R_L \leq 0.05$, respectively (medians were 23.6 and 16.6
127 times higher). These results presented the reasonability of using R_L as proxy for terrestrial
128 transport.

129   In addition to AEC and R_L, the harmonic mean of BLH along trajectory (BLH_traj) and
130 the retention ratio of air mass within MBL (R_{MBL}) were also calculated (Zhou et al., 2021).

131   2.2 Analysis of Spatiotemporal Variation

132   Our research domain (23−37° N, 117−130° E) includes the south Yellow Sea (YS), the
133 East China Sea (ECS) and part of Northwest Pacific (NP). It was divided into 145 $1° \times 1°$ grids
134 as shown in Figure S2. In order to reveal the spatiotemporal variations of AEC and R_L in this
135 region, trajectories starting from the center of each grid were calculated with an interval of 6
136 hours during 1 January 2009 to 31 December 2020, and a total of 17532 trajectories were
137 obtained for each grid. Then the R_L, AEC, BLH_traj (further divided to BLH_L and BLH_O for
138 endpoints located over the land and ocean, respectively), R_{MBL} and AEC* (AEC index without the
139 BLH term) indexes corresponding to each trajectory were calculated. Empirical orthogonal
140 function (EOF) analysis, a widely used approach to extract the spatially and temporally varying
141 modes from climate variables, was used to decompose the AEC and R_L monthly anomalies (144
142 $\times$ 145 matrixes). The principle and calculation method of EOF analysis can be found in Li et al.
143 (2013).

144   2.3 Field Observations and Parameterization of Marine Biogenic MSA

145   Total suspended particulate (TSP) samples were collected by high-volume samplers in a
146   total of 6 cruises in the eastern China seas during 2014 to 2020. The concentrations of water-
147   soluble ions, including MSA, were determined by ion chromatography (IC) and trace metals
148   were determined by inductively coupled plasma mass spectrometry (ICP-MS). The details about
149   the cruise campaigns and aerosol measurements are given in Text S1 and Figure S3. Previously
150   reported data of aerosol MSA from 2 islands (Huaniao Island 30.9° N, 122.7° E; and Okinawa
151   Island 26.9° N, 128.2° E) and 8 cruise campaigns during 2009 to 2020 were also integrated for
152   parameterization. The detailed locations, time periods, and data sources are listed in Table S1.

153   The entire research domain was split into three regions (Region 1 to Region 3) based on
154   monthly averaged AEC dataset from 2009 to 2020 using the K-means clustering algorithm
155   (shown in Figure 2b). The K-means clustering divide the initial dataset into a predefined number
156   of subgroups by minimizing the sum of squared Euclidean distances between each data point and
157   the corresponding cluster centers (Beddows et al., 2014). The data match-up between AEC and
158   the concentration of marine biogenic MSA was performed for each region (see details in Text
159   S2), and the linear regression functions between two variables were obtained. Using the
160   parameterization scheme between MSA and AEC, the spatiotemporal distribution of marine
161   biogenic MSA was simulated. For grids located on the boundary, the fitting parameters were
162   obtained by linearly interpolating the parameters of two adjacent regions.

163   **3 Results and Discussion**

164   3.1 Spatiotemporal Distribution of AEC

165   According to previous study, the linkage between aerosol components and AEC could be
166   established when marine air mass transported mainly within the boundary layer (Zhou et al.,
167   2021). Therefore, the AEC and other indexes were filtrated by the condition of $R_{MBL} > 0.9$ in this
168   study. The AEC generally decreased from the northwest to southeast oceanic regions with the
169   highest values occurring in the majority of YS and coastal ECS in April and May, and the lowest
170   indexes distributed in the NP especially in summer (Figure S4).

171   The EOF analysis of AEC showed that the first mode (Mode 1) could explain 77.3% of
172   variance and decreased from the YS and northern coastal ECS to the remote ocean (Figure 1a).
173   The corresponding principal component (PC1) demonstrated an annual cycle with the maximum
174   in April and May and the minimum during November to January as well as an inter-annual
175   variation with relatively high values in 2015–2017 (Figure 1b). Both spatial and seasonal
176   variations of Mode 1 were co-controlled by surface Chl *a* and BLH. Specifically, higher values
177   in the YS and coastal ECS generally accorded with higher Chl *a* concentrations and lower BLH
178   (Figures S5–S7), and PC1 peaked in the late spring every year corresponding to almost each
179   spike of Chl *a* (spring bloom) and trough of BLH (Figure 1b). The seasonal variation of BLH
180   over the ECS was suggested to be affected by thermal stability defined as sea surface
181   temperature minus the temperature at 850 hPa (Kuribayashi et al., 2011). The inter-annual
182   variation of PC1 seemed predominantly driven by the BLH and its highest peaks in 2015–2017
183   were likely associated with the decreasing troughs of BLH during 2009 to 2016 and the increase
184   afterwards (Figure 1b).

185　　　　　The second mode (Mode 2) explained 5.3% of overall variance. Its variation in the
186　western YS and coastal ECS was opposite to the open ECS and NP (Figure 1a), which was likely
187　caused by the distinct Chl *a* phenology in different regions. Due to the strong stratification
188　limiting nutrient availability in the surface water and strong grazing pressure by
189　microzooplankton (Guo et al., 2014; Liu et al., 2019), the concentration of surface Chl *a* in open
190　ECS and NP reached the minimum in summer (Figure S5). But in coastal seas, the nutrient input
191　from rivers and upwelling in summer sustained the phytoplankton biomass at a high level (Liu et
192　al., 2019; Yamaguchi et al., 2013). Mode 2 dominated the seasonal variation of AEC in the
193　remote ocean, and the time series of corresponding principle component (PC2) exhibited the
194　minimum in summer (Figure 1b).

195　　　　　It should be noted that the highest Chl *a* along the coast especially in the outer Yangtze
196　River Estuary is not reproduced by the distribution of AEC or AEC[*] (Figures S4–S6). It reflects
197　the mismatch between local and air mass exposed Chl *a* concentrations. Accordingly, previous
198　studies have indicated that variations of aerosol components cannot be linked to local surface Chl
199　*a* synchronously and certain time lags exist for linking regional Chl *a* (Mansour et al., 2020a;
200　Mansour et al., 2020b; Rinaldi et al., 2013). The AEC index, with more concrete characterization
201　on the exposure of air mass to marine biogenic emission along air transport path, is likely to
202　better connect with marine biogenic aerosols at the receptor site. Near-surface wind speed and
203　sea surface temperature (SST), two factors affecting the sea-to-air fluxes of gases and sea spray
204　aerosols (de Leeuw et al., 2011; Liss and Merlivat, 1986), are not considered in our AEC
205　calculation. This may impact the abovementioned performance of AEC as an indicator for
206　marine biological source. However, the effect of wind speed may be averaged out as obtaining
207　the variation on a monthly resolution (Spracklen et al., 2008) and SST influence is much weaker
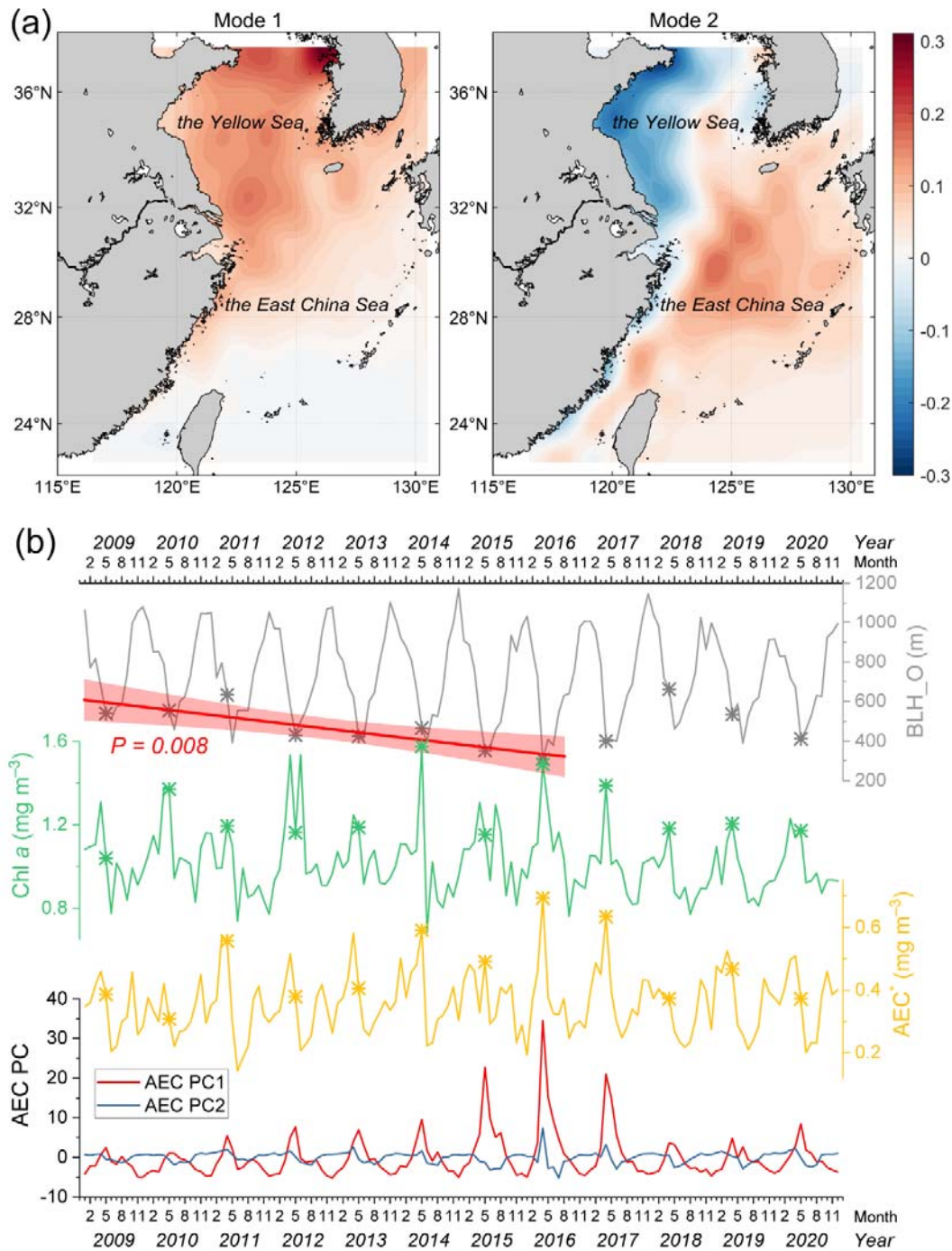208　than wind speed (Land et al., 2014; Li et al., 2019).

Figure 1. Spatiotemporal variation of air mass exposure to chlorophyll a (AEC) index and its controlling factors. (a) The first two EOF modes of AEC anomalies during 2009 to 2020. (b) Time series of principal components (PC) corresponding to the first teo EOF modes and monthly averages of AEC* value, Chl a concentration, and boundary layer height (BLH) along trajectories over the ocean (BLH_O) during 2009 to 2020. Note that AEC, AEC* and BLH_O were all filtrated by the condition of $R_{MBL} > 0.9$ (within marine boundary layer). The stars in series of AEC*, Chl a, and BLH_O correspond to the month in which the AEC PC1 reaches the

217 highest each year. The red line and shaded region in top panel represent the linear regression and
218 corresponding 95% confidence interval for BLH_O at peak-AEC month between 2009 and 2016.

219 ### 3.2 Simulation of Marine Biogenic MSA

220 Under the condition of $R_{MBL} > 0.9$, a significant correlation was found between aerosol
221 MSA and the AEC index during the spring and summer but not in the autumn and winter over
222 the eastern China seas (Figure S8). Correspondingly, MSA was not correlated with non-sea-salt
223 SO_4^{2-} (nss-SO_4^{2-}) and the ratio of MSA to nss-SO_4^{2-} (MSA/nss-SO_4^{2-}) was significantly lower
224 under high R_L regime than with low R_L during the spring and summer, while opposite
225 phenomena existed in the autumn and winter (Figures S8–S9). This suggested that the conclusion
226 drawn from the coastal island (MSA is dominantly from marine biogenic source in spring and
227 summer but largely contributed by terrestrial transport in autumn and winter, (Zhou et al., 2021)
228 might be applicable to the entire eastern China seas. Thus, the potential impacts of terrestrial
229 MSA needs to be screened out when doing the data match-up (Text S2). Extremely low fraction
230 of terrestrial air mass in summer (Figure 3a) and high biogenic emission in spring (Figure S4)
231 can explain the dominance of biogenic MSA in these two seasons.

232 Considering the large spatial disparities in the variation and controls of AEC, and the
233 emission rate of DMS related to phytoplankton community, temperature, radiation, mixed layer
234 depth, etc. (Stefels et al., 2007; Vallina and Simó, 2007) from the coastal seas to open ocean, the
235 research domain was divided into three regions by K-means clustering (Section 2.3.). The mean
236 AEC value decreased from Region 1 to Region 3 with its peak time advancing from May to
237 April (Figure S10). The seasonal variation of AEC in Region 1 was in accordance with marine
238 biogenic MSA (filtrated by $R_L < 0.1$) over Huaniao Island, which was the highest in spring,
239 followed by summer and then autumn and winter (Zhou et al., 2021). The seasonal change of
240 AEC in Region 3 was consistent with the MSA observations over Okinawa Island and AEC PC2,
241 showing the highest in spring and lowest in summer (Kunwar and Kawamura, 2014; Zhu et al.,
242 2015). These results verified the feasibility of using AEC to infer the variation of marine
243 biogenic MSA.

244 After data match-up and binning, good correlations were found between marine biogenic
245 MSA and AEC for all three regions (Figure 2a). The linear fitting slope increased in the order of
246 Region 1 < Region 2 < Region 3, which was opposite to the order of mean AEC. These linear
247 regression functions could serve as a parameterization scheme for simulating the distribution of
248 marine biogenic MSA between 2009 to 2020 (Figure 2b). It was found that the highest oceanic
249 MSA concentrations appeared in April and May over Region 2, exceeding 0.1 μg m^{-3} (Figure 2b-
250 c). According to historical observations, mean MSA concentration in spring over Region 1 (~
251 0.050 μg m^{-3}) was lower than that over Region 2 (~ 0.065 μg m^{-3}), and this spatial characteristic
252 was reproduced by the simulation. In summer, the MSA concentrations over the YS and coastal
253 area (Region 1) were higher than other regions. However, in autumn and winter, the hot spot
254 relocated to Region 3 probably due to high formation efficiency of aerosol MSA. Overall, the
255 difference of marine biogenic MSA concentration among three regions was much lower than that
256 of AEC value.

257 Four cruises during 2006 to 2007 over the northern YS (adjacent to Region 1) measured
258 average MSA concentrations of 0.073, 0.039, 0.011, and 0.015 μg m^{-3} in spring (April – May),
259 summer (July – August), autumn (October), and winter (January), respectively (Zhang and Yang,
260 2009; Zhang, 2009). The seasonal variation and concentration levels were similar to those of

261 simulated MSA in Region 1, except for slightly higher concentration in winter than in autumn
262 likely associated with more terrestrial transport. MSA concentration over Jeju Island during 2001
263 to 2002 peaked in spring, with a seasonal mean of 0.066 μg m^{-3} similar to our estimates for
264 Region 2 (0.074 μg m^{-3}) (Tyagi et al., 2017). The simulation of aerosol MSA over the eastern
265 China seas by atmospheric chemical transport model (CTM) is scarce. Li et al. (2020) explored
266 the atmospheric chemistry of oceanic DMS in this region via WRF-CMAQ model, but only the
267 distribution of gas-phase MSA was provided, showing the highest in summer. The model did not
268 incorporate aqueous-phase oxidation pathways, which could be the dominant mechanism of
269 MSA formation (Hoffmann et al., 2016). As a result, large uncertainties may exist in the CTM
270 simulating results. By contrast, our results inferred from the AEC index and constrained by
271 observations could well capture the spatiotemporal distribution pattern of marine biogenic MSA
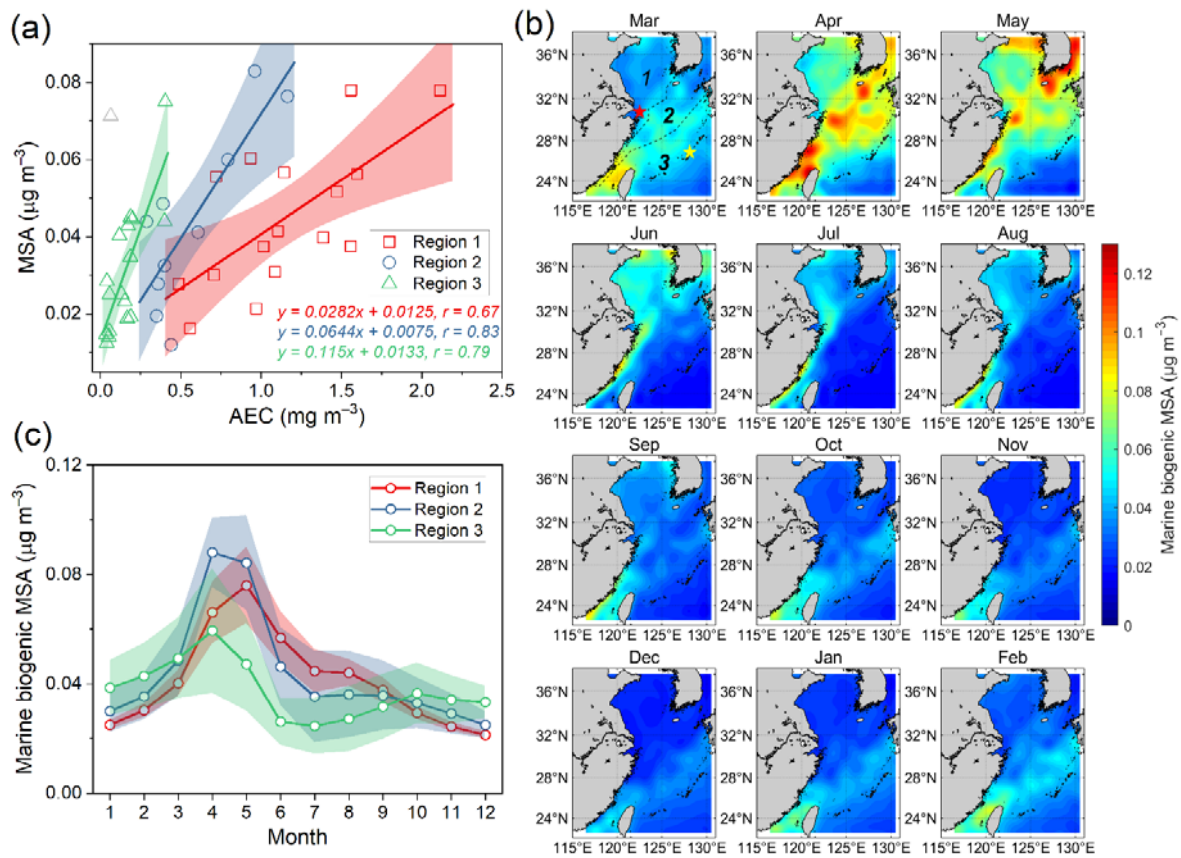272 in aerosols.

273

274 **Figure 2**. Parameterized simulation of spatiotemporal distribution of marine biogenic MSA. (a)
275 Correlations between measured particulate MSA concentration and AEC index in each region.
276 One data point of Region 3 (the gray triangle) was excluded from the correlation analysis. The
277 shaded regions represent the 95% confidence interval of linear regression. (b) Monthly
278 climatology of simulated marine biogenic MSA. Dashed lines show the boundaries among three
279 regions. Red and yellow stars represent the location of Huaniao Island and Okinawa Island,

280 respectively. (c) The average concentrations of simulated marine biogenic MSA for each region
281 in different months. The shaded band denotes the mean ± SD for each region.

282   3.3 Significance of marine biogenic source relative to terrestrial transport

283   Eastern China seas is significantly influenced by terrestrial transport, which may greatly
284 weaken the relative importance of marine biogenic source to aerosols. The extent of terrestrial
285 influence exhibited a decreasing trend from offshore to the remote ocean (YS > ECS > NP) and a
286 significant seasonal variation (winter > spring and autumn > summer) (Figure 3a). The EOF
287 analysis of R_L anomalies showed that Mode 1 explained 90.7% of total variance and exhibited
288 identical signs over the entire studied region (Figure 3b), clearly showing the uniform control of
289 East Asian monsoon. The R_L values over the ECS and NP were mostly below 0.1 in summer (Jun
290 to August), suggesting extremely low terrestrial influence with prevailing southeast wind (Figure
291 1a). In this case, marine biogenic emission could be an important contributor to submicron
292 organic aerosols and greatly affect radiative forcing.

293   As for winter, the intensity of terrestrial transport presented a significant decadal decrease
294 (Figure 3c, $P < 0.05$) as the highest monthly mean and three-month (November, December, and
295 January next year) mean of R_L during 2015 to 2020 dropped approximately 13.4% and 9.2%
296 compared to the period of 2009 to 2014, respectively. This decadal decrease was likely caused
297 by the weakening of East Asian winter monsoon after 1980s, influenced by large-scale climatic
298 factors such as warming of NP (Pei et al., 2018), loss of Arctic sea-ice in autumn and extensive
299 boreal snowfall in the earlier winter (Zou et al., 2017), variation of quasi-stationary planetary
300 wave activity (Kang et al., 2009), and significant winter warming in northern China (Xu et al.,
301 2006).

302   In the recent decade, China execute remarkable cut-down on air pollutant emissions. For
303 example, SO_2 declined approximately 62% from 2010 to 2017 (Zheng et al., 2018) and thereby
304 its outflow flux to the eastern China seas probably decreased by a larger fraction by integrating
305 the change of R_L. Meanwhile, ship emission also dropped sharply due to the improvement of fuel
306 oil quality with the establishment of Domestic Emission Control Areas and the implementation
307 of "IMO 2020 regulation" (Yu et al., 2021; Zou et al., 2020). By contrast, no obvious decrease
308 was found in the decadal changes of Chl a and AEC in the eastern China seas (Figure 1b),
309 suggesting the elevated importance of marine biogenic source to aerosol components in this
310 region (for example, sulfate and OC both related to MSA). For example, the MSA/nss-SO_4^{2-}
311 during 2016–2018 was 1.4 times higher than that during 2013–2015 over Huaniao Island (Zhou
312 et al., 2021). Considering the concurrent decline of terrestrial MSA, the ratio of biogenic MSA to
313 nss-SO_4^{2-} was likely to exhibited a higher increase degree. Previous studies reported that average
314 MSA/nss-SO_4^{2-} ratios over the eastern China seas were 0.00074 and 0.0038 in the winter of 2009
315 and summer of 2011, respectively (He et al., 2011; Zhang et al., 2014). Based on our cruise
316 observations, the ratios reached 0.0057 and 0.018 in the winter of 2019 and summer of 2018,
317 suggesting that fractional contribution of marine biogenic source to nss-SO_4^{2-} may have
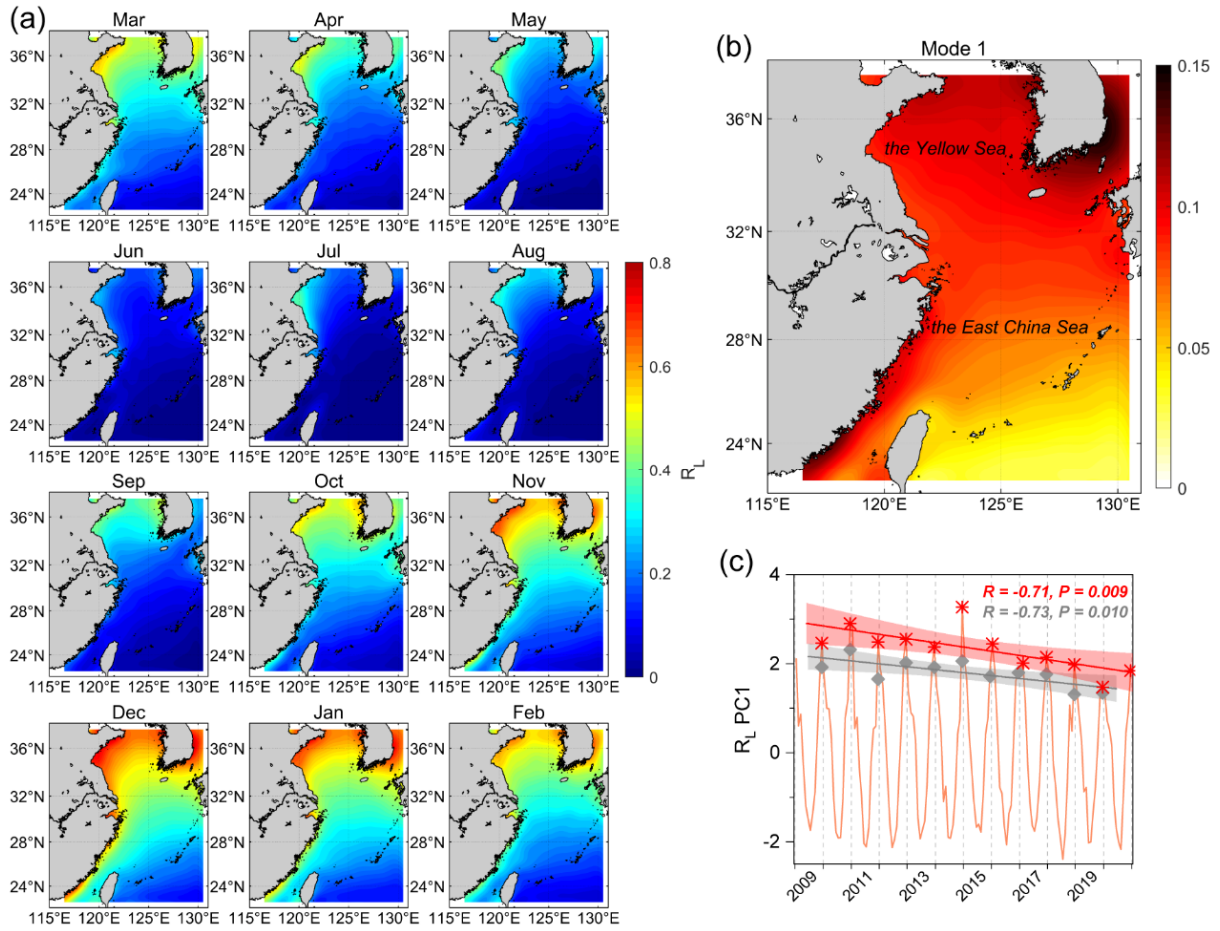318 increased by over 5 times during this period.

Figure 3. (a) Monthly climatology of R_L distribution during 2009–2020. (b) The first EOF mode of R_L monthly anomalies and (c) the time series of corresponding principal component (R_L PC1) during 2009–2020. The red star and gray diamond represent the highest monthly mean and the mean of November, December and January next year of R_L PC1, respectively. The linear lines and associated shaded bands show the linear regressions and their 95% confidence intervals.

4 Conclusions

Marine biogenic emissions from the eastern China seas may contribute significantly to atmospheric aerosols in spring and summer, and its fractional contribution exhibits a possibly decadal increase with the weakening of wintertime terrestrial transport and dramatic decrease of anthropogenic emissions. The AEC index quantifies how air masses are exposed to marine biogenic source during the transport. Using AEC as an indicator, this study investigates the 12-year spatiotemporal variations of the influence extent of marine biogenic emissions on boundary layer, which showed the highest in spring, and the lowest in winter for the YS and coastal ECS and in summer for the remote ocean, respectively. The spatial and seasonal patterns were co-controlled by surface phytoplankton biomass and BLH along the transport path, and the inter-annual change was predominantly associated with BLH.

The seasonal variations of calculated AEC value are generally consistent with measured MSA concentrations at the same region. By integrating aerosol MSA data observed on 14 cruises

338 and 2 islands, an AEC-based parameterization scheme was constructed and applied to simulate
339 the spatiotemporal distribution of marine biogenic MSA. Although there are uncertainties in the
340 empirical simulation results, this observation-constrained approach provides a different
341 perspective for obtaining the distribution of biogenic sulfur in the atmosphere, particularly in the
342 context that chemical mechanisms in CTMs are still less comprehensive (Li et al., 2020; Veres et
343 al., 2020). Similar methods can also be applied to other marine biogenic components in the
344 aerosol (Sanchez et al., 2021), especially for those relatively stable during the transport. The
345 AEC calculation can also be improved by replacing Chl *a* concentration with other parameters
346 more closely related to the aerosol component (e.g. sea surface DMS for biogenic sulfur
347 aerosols) or adding other influencing factors like SST and radiation. Our study provides
348 enlightenment on linking aerosol components and properties to marine biological activities and
349 exploring the role of phytoplankton in potential ocean-aerosol-climate feedback with the
350 perturbation of anthropogenic forcing.

351

362

Open Research

364 The GDAS meteorological dataset can be accessed at ftp://ftp.arl.noaa.gov/pub/archives/gdas1.
365 The remote-sensing Chl *a* datasets are available at https://oceandata.sci.gsfc.nasa.gov/. The
366 aerosol measurement data during four 4 cruises (2017-2020) in the eastern China seas and
367 corresponding indices (AEC, R_L, and R_{MBL}) are available at
368 https://doi.org/10.5281/zenodo.7057317 (Zhou et al., 2022). Arranged data for constructing the
369 parameterization scheme were listed in Table S1. All calculated 6-hour gridded data (AEC,
370 AEC*, R_L, R_{MBL}, BLH_traj, BLH_L, BLH_O) and related Matlab code have been deposited in
371 https://doi.org/10.5281/zenodo.7056981 (Zhou and Chen, 2022). The M_Map toolbox is publicly
372 available at https://www.eoas.ubc.ca/~rich/map.html (Pawlowicz, 2020).

373

374

References

376 Arnold, S. R., Spracklen, D. V., Gebhardt, S., Custer, T., Williams, J., Peeken, I., and Alvain, S.

(2010), Relationships between atmospheric organic compounds and air-mass exposure to marine biology, *Environmental Chemistry*, *7*(3), 232-241, doi:10.1071/en09144.

Beddows, D. C. S., Dall'Osto, M., Harrison, R. M., Kulmala, M., Asmi, A., Wiedensohler, A., et al. (2014), Variations in tropospheric submicron particle size distributions across the European continent 2008–2009, *Atmospheric Chemistry and Physics*, *14*(8), 4327-4348, doi:10.5194/acp-14-4327-2014.

Blazina, T., Laderach, A., Jones, G. D., Sodemann, H., Wernli, H., Kirchner, J. W., and Winkel, L. H. (2017), Marine Primary Productivity as a Potential Indirect Source of Selenium and Other Trace Elements in Atmospheric Deposition, *Environmental Science & Technology*, *51*(1), 108-118, doi:10.1021/acs.est.6b03063.

Carpenter, L. J., Archer, S. D., and Beale, R. (2012), Ocean-atmosphere trace gas exchange, *Chemical Society Reviews*, *41*(19), 6473-6506, doi:10.1039/c2cs35121h.

de Leeuw, G., Andreas, E. L., Anguelova, M. D., Fairall, C. W., Lewis, E. R., O'Dowd, C., et al. (2011), Production flux of sea spray aerosol, *Reviews of Geophysics*, *49*(2), 2010RG000349, doi:10.1029/2010rg000349.

Facchini, M. C., Decesari, S., Rinaldi, M., Carbone, C., Finessi, E., Mircea, M., et al. (2008), Important source of marine secondary organic aerosol from biogenic amines, *Environmental Science & Technology*, *42*(24), 9116-9121, doi:10.1021/es8018385.

Guo, C., Liu, H., Zheng, L., Song, S., Chen, B., and Huang, B. (2014), Seasonal and spatial patterns of picophytoplankton growth, grazing and distribution in the East China Sea, *Biogeosciences*, *11*(7), 1847-1862, doi:10.5194/bg-11-1847-2014.

Guo, T., Li, K., Zhu, Y., Gao, H., and Yao, X. (2016), Concentration and size distribution of particulate oxalate in marine and coastal atmospheres – Implication for the increased importance of oxalate in nanometer atmospheric particles, *Atmospheric Environment*, *142*, 19-31, doi:10.1016/j.atmosenv.2016.07.026.

He, Y., Yang, G., and Zhang, H. (2011), Composition and source of atmosphere aerosol water soluble ions over the East China Sea in winter, *Environmental Science*, *32*(8), 2197-2203, doi:10.13227/j.hjkx.2011.08.034. *In Chinese*.

Hoffmann, E. H., Tilgner, A., Schroedner, R., Bräuer, P., Wolke, R., and Herrmann, H. (2016), An advanced modeling study on the impacts and atmospheric implications of multiphase dimethyl sulfide chemistry, *Proceedings of the National Academy of Sciences of the United States of America*, *113*(42), 11776-11781, doi:10.1073/pnas.1606320113.

Hu, Q., Yu, P., Zhu, Y., Li, K., Gao, H., and Yao, X. (2015), Concentration, Size Distribution, and Formation of Trimethylaminium and Dimethylaminium Ions in Atmospheric Particles over Marginal Seas of China, *Journal of the Atmospheric Sciences*, *72*(9), 3487-3498, doi:10.1175/jas-d-14-0393.1.

Kang, L., Chen, W., Gu, L., Huang, R., and Wang, L. (2009), Interdecadal Variations of the East Asian Winter Monsoon and Their Association with Quasi-Stationary Planetary Wave Activity, *Journal of Climate*, *22*(18), 4860-4872, doi:10.1175/2009jcli2973.1.

Kunwar, B., and Kawamura, K. (2014), One-year observations of carbonaceous and nitrogenous components and major ions in the aerosols from subtropical Okinawa Island, an outflow region of

Asian dusts, *Atmospheric Chemistry and Physics*, *14*(4), 1819-1836.

Kuribayashi, M., Ohara, T., and Shimizu, A. (2011), Temporal variation and vertical structure of the marine atmospheric mixed layer over the East China Sea from Mie-scattering lidar data, *Sola*, *7*, 189-192.

Land, P. E., Shutler, J. D., Bell, T. G., and Yang, M. (2014), Exploiting satellite earth observation to quantify current global oceanic DMS flux and its future climate sensitivity, *Journal of Geophysical Research: Oceans*, *119*(11), 7725-7740, doi:10.1002/2014jc010104.

Li, H., Qin, X., Wang, G., Xu, J., Wang, L., Lu, D., et al. (2022), Conjoint impacts of continental outflows and marine sources on brown carbon in the East China sea: Abundances, optical properties, and formation processes, *Atmospheric Environment*, *273*, doi:10.1016/j.atmosenv.2022.118959.

Li, J., Carlson, B. E., and Lacis, A. A. (2013), Application of spectral analysis techniques in the intercomparison of aerosol data: 1. An EOF approach to analyze the spatial-temporal variability of aerosol optical depth using multiple remote sensing data sets, *Journal of Geophysical Research: Atmospheres*, *118*(15), 8640-8648, doi:10.1002/jgrd.50686.

Li, S., Zhang, Y., Zhao, J., Sarwar, G., Zhou, S., Chen, Y., et al. (2020), Regional and Urban-Scale Environmental Influences of Oceanic DMS Emissions over Coastal China Seas, *Atmosphere*, *11*(8), doi:10.3390/atmos11080849.

Li, Y., He, Z., Yang, G.-P., Wang, H., and Zhuang, G.-C. (2019), Volatile halocarbons in the marine atmosphere and surface seawater: Diurnal and spatial variations and influences of environmental factors, *Atmospheric Environment*, *214*, 116820, doi:10.1016/j.atmosenv.2019.116820.

Liss, P. S., and Merlivat, L. (1986), Air-Sea Gas Exchange Rates: Introduction and Synthesis, *The Role of Air-Sea Exchange in Geochemical Cycling*, *185*, 113-127.

Liu, X., Laws, E. A., Xie, Y., Wang, L., Lin, L., and Huang, B. (2019), Uncoupling of Seasonal Variations Between Phytoplankton Chlorophyll a and Production in the East China Sea, *Journal of Geophysical Research: Biogeosciences*, *124*(7), 2400-2415, doi:10.1029/2018jg004924.

Mansour, K., Decesari, S., Bellacicco, M., Marullo, S., Santoleri, R., Bonasoni, P., et al. (2020a), Particulate methanesulfonic acid over the central Mediterranean Sea: Source region identification and relationship with phytoplankton activity, *Atmospheric Research*, *237*, 104837, doi:10.1016/j.atmosres.2019.104837.

Mansour, K., Decesari, S., Facchini, M. C., Belosi, F., Paglione, M., Sandrini, S., et al. (2020b), Linking Marine Biological Activity to Aerosol Chemical Composition and Cloud‐Relevant Properties Over the North Atlantic Ocean, *Journal of Geophysical Research: Atmospheres*, *125*(13), e2019JD032246, doi:10.1029/2019jd032246.

O'dowd, C. D., Facchini, M. C., Cavalli, F., Ceburnis, D., Mircea, M., Decesari, S., et al. (2004), Biogenically driven organic contribution to marine aerosol, *Nature*, *431*(7009), 676, doi:10.1038/nature02959.

Park, K.-T., Jang, S., Lee, K., Yoon, Y. J., Kim, M.-S., Park, K., et al. (2017), Observational evidence for the formation of DMS-derived aerosols during Arctic phytoplankton blooms, *Atmospheric Chemistry and Physics*, *17*(15), 9665-9675, doi:10.5194/acp-17-9665-2017.

Park, K.-T., Lee, K., Kim, T.-W., Yoon, Y. J., Jang, E.-H., Jang, S., et al. (2018), Atmospheric DMS

in the Arctic Ocean and Its Relation to Phytoplankton Biomass, *Global Biogeochemical Cycles*, *32*(3), 351-359, doi:10.1002/2017gb005805.

Pawlowicz, R. (2020), M_Map: A mapping package for MATLAB (Version 1.4m) [Software]. https://www.eoas.ubc.ca/~rich/map.html.

Pei, L., Yan, Z., Sun, Z., Miao, S., and Yao, Y. (2018), Increasing persistent haze in Beijing: potential impacts of weakening East Asian winter monsoons associated with northwestern Pacific sea surface temperature trends, *Atmospheric Chemistry and Physics*, *18*(5), 3173-3183, doi:10.5194/acp-18-3173-2018.

Pöschl, U. (2005), Atmospheric aerosols: composition, transformation, climate and health effects, *Angewandte Chemie International Edtion in English*, *44*(46), 7520-7540, doi:10.1002/anie.200501122.

Rinaldi, M., Fuzzi, S., Decesari, S., Marullo, S., Santoleri, R., Provenzale, A., et al. (2013), Is chlorophyll-a the best surrogate for organic matter enrichment in submicron primary marine aerosol?, *Journal of Geophysical Research: Atmospheres*, *118*(10), 4964-4973, doi:10.1002/jgrd.50417.

Sanchez, K. J., Zhang, B., Liu, H., Saliba, G., Chen, C.-L., Lewis, S. L., et al. (2021), Linking marine phytoplankton emissions, meteorological processes, and downwind particle properties with FLEXPART, *Atmospheric Chemistry and Physics*, *21*(2), 831-851, doi:10.5194/acp-21-831-2021.

Savoie, D. L., Arimoto, R., Keene, W. C., Prospero, J. M., Duce, R. A., and Galloway, J. N. (2002), Marine biogenic and anthropogenic contributions to non-sea-salt sulfate in the marine boundary layer over the North Atlantic Ocean, *Journal of Geophysical Research*, *107*(D18), 4356, doi:10.1029/2001jd000970.

Spracklen, D. V., Arnold, S. R., Sciare, J., Carslaw, K. S., and Pio, C. (2008), Globally significant oceanic source of organic carbon aerosol, *Geophysical Research Letters*, *35*(12), L12811, doi:10.1029/2008gl033359.

Stefels, J., Steinke, M., Turner, S., Malin, G., and Belviso, S. (2007), Environmental constraints on the production and removal of the climatically active gas dimethylsulphide (DMS) and implications for ecosystem modelling, *Biogeochemistry*, *83*(1-3), 245-275, doi:10.1007/s10533-007-9091-5.

Tyagi, P., Kawamura, K., Kariya, T., Bikkina, S., Fu, P., and Lee, M. (2017), Tracing atmospheric transport of soil microorganisms and higher plant waxes in the East Asian outflow to the North Pacific Rim by using hydroxy fatty acids: Year-round observations at Gosan, Jeju Island, *Journal of Geophysical Research: Atmospheres*, *122*(7), 4112-4131, doi:10.1002/2016jd025496.

Vallina, S. M., and Simó, R. (2007), Strong relationship between DMS and the solar radiation dose over the global surface ocean, *Science*, *315*(5811), 506-508, doi:10.1126/science.1133680.

Veres, P. R., Neuman, J. A., Bertram, T. H., Assaf, E., Wolfe, G. M., Williamson, C. J., et al. (2020), Global airborne sampling reveals a previously unobserved dimethyl sulfide oxidation mechanism in the marine atmosphere, *Proceedings of the National Academy of Sciences of the United States of America*, *117*(9), 4505-4510, doi:10.1073/pnas.1919344117.

Wang, F., Chen, Y., Meng, X., Fu, J., and Wang, B. (2016), The contribution of anthropogenic sources to the aerosols over East China Sea, *Atmospheric Environment*, *127*, 22-33,

doi:10.1016/j.atmosenv.2015.12.002.

Xu, L., Liu, X. H., Gao, H. W., Yao, X. H., Zhang, D. Z., Bi, L., et al. (2021), Long-range transport of anthropogenic air pollutants into the marine air: insight into fine particle transport and chloride depletion on sea salts, *Atmospheric Chemistry and Physics*, *21*(23), 17715-17726, doi:10.5194/acp-21-17715-2021.

Xu, M., Chang, C.-P., Fu, C., Qi, Y., Robock, A., Robinson, D., and Zhang, H.-m. (2006), Steady decline of east Asian monsoon winds, 1969–2000: Evidence from direct ground measurements of wind speed, *Journal of Geophysical Research*, *111*(D24), D24111, doi:10.1029/2006jd007337.

Yamaguchi, H., Ishizaka, J., Siswanto, E., Baek Son, Y., Yoo, S., and Kiyomoto, Y. (2013), Seasonal and spring interannual variations in satellite-observed chlorophyll-a in the Yellow and East China Seas: New datasets with reduced interference from high concentration of resuspended sediment, *Continental Shelf Research*, *59*, 1-9, doi:10.1016/j.csr.2013.03.009.

Yang, G.-P., Zhang, H.-H., Su, L.-P., and Zhou, L.-M. (2009), Biogenic emission of dimethylsulfide (DMS) from the North Yellow Sea, China and its contribution to sulfate in aerosol during summer, *Atmospheric Environment*, *43*(13), 2196-2203, doi:10.1016/j.atmosenv.2009.01.011.

Yu, G., Zhang, Y., Yang, F., He, B., Zhang, C., Zou, Z., et al. (2021), Dynamic Ni/V Ratio in the Ship-Emitted Particles Driven by Multiphase Fuel Oil Regulations in Coastal China, *Environmental Science & Technology*, *55*(22), 15031-15039, doi:10.1021/acs.est.1c02612.

Zhang, H.-H., and Yang, G.-P. (2009), Biogenic emission of dimethylsulfide (DMS) from the North Yellow Sea and its contribution to non-sea-salt sulfate in aerosol, *Periodical of Ocean University of China*, *4*, 1672-5174. *In Chinese*.

Zhang, H. (2009), Stuides on Biogeochemistry of DMS and DMSP in the East China Sea and the Yellow Sea, PhD thesis, Ocean University of China. *In Chinese*.

Zhang, S. H., Yang, G. P., Zhang, H. H., and Yang, J. (2014), Spatial variation of biogenic sulfur in the south Yellow Sea and the East China Sea during summer and its contribution to atmospheric sulfate aerosol, *Science of the Total Environment*, *488-489*, 157-167, doi:10.1016/j.scitotenv.2014.04.074.

Zheng, B., Tong, D., Li, M., Liu, F., Hong, C., Geng, G., et al. (2018), Trends in China's anthropogenic emissions since 2010 as the consequence of clean air actions, *Atmospheric Chemistry and Physics*, *18*(19), 14095-14111, doi:10.5194/acp-18-14095-2018.

Zhou, S., and Chen, Y. (2022), Air mass exposure to chlorophyll a (AEC) over the eastern China seas (Version 1.0) [Dataset]. Zenodo. https://doi.org/10.5281/zenodo.7056981.

Zhou, S., Chen, Y., Paytan, A., Li, H., Wang, F., Zhu, Y., et al. (2021), Non‐Marine Sources Contribute to Aerosol Methanesulfonate Over Coastal Seas, *Journal of Geophysical Research: Atmospheres*, *126*(21), e2021JD034960, doi:10.1029/2021jd034960.

Zhou, S., Chen, Y., Wang, F., Bao, Y., Ding, X., and Xu, Z. (2022), Aerosol measurements over the eastern China seas during 2017 to 2020 [Dataset]. Zenodo. https://doi.org/10.5281/zenodo.7057317.

Zhou, S., Li, H., Yang, T., Chen, Y., Deng, C., Gao, Y., et al. (2019), Characteristics and sources of aerosol aminiums over the eastern coast of China: insights from the integrated observations in a

coastal city, adjacent island and surrounding marginal seas, *Atmospheric Chemistry and Physics*, *19*(16), 10447-10467, doi:10.5194/acp-19-10447-2019.

Zhu, C., Kawamura, K., and Kunwar, B. (2015), Organic tracers of primary biological aerosol particles at subtropical Okinawa Island in the western North Pacific Rim, *Journal of Geophysical Research: Atmospheres*, *120*(11), 5504-5523, doi:10.1002/2015jd023611.

Zou, Y., Wang, Y., Zhang, Y., and Koo, J. H. (2017), Arctic sea ice, Eurasia snow, and extreme winter haze in China, *Science Advances*, *3*(3), e1602751, doi:10.1126/sciadv.1602751.

Zou, Z., Zhao, J., Zhang, C., Zhang, Y., Yang, X., Chen, J., et al. (2020), Effects of cleaner ship fuels on air quality and implications for future policy: A case study of Chongming Ecological Island in China, *Journal of Cleaner Production*, *267*, doi:10.1016/j.jclepro.2020.122088.

References From the Supporting Information

Fu, J., B. Wang, Y. Chen, and Q. Ma (2018), The influence of continental air masses on the aerosols and nutrients deposition over the western North Pacific, *Atmospheric Environment*, *172*, 1-11, doi:10.1016/j.atmosenv.2017.10.041.

He, Y. (2011), Composition and Sorce of Atmosphere Aerosol Water Soluble Ions over the China Coastal Seas, Master thesis, Ocean University of China. *In Chinese.*

Ji, J., L. Chen, J. Wang, H. Lin, and Q. Lin (2016), Characters of the aerosol over the northwest Pacific and eastern China coastal area in autumn, *Journal of Applied Oceanography*, *35*(3), 339-347, doi:10.3969/J.ISSN.2095-4972.2016.03.004. *In Chinese.*

Pilson, M. E. (2012), *An Introduction to the Chemistry of the Sea*, Cambridge University Press.

Xue, L. (2012), Temporal-spatial Variations and Chemical Characteristics of Atmospheric Aerosol over the East China Marginal Seas, Master thesis, Ocean University of China. *In Chinese.*

Yang, T., Y. Chen, S. Zhou, H. Li, F. Wang, and Y. Zhu (2020), Solubilities and deposition fluxes of atmospheric Fe and Cu over the Northwest Pacific and its marginal seas, *Atmospheric Environment*, *239*, 117763, doi:10.1016/j.atmosenv.2020.117763.

Zhang, S. H., G. P. Yang, H. H. Zhang, and J. Yang (2014), Spatial variation of biogenic sulfur in the south Yellow Sea and the East China Sea during summer and its contribution to atmospheric sulfate aerosol, *Science of the Total Environment*, *488-489*, 157-167, doi:10.1016/j.scitotenv.2014.04.074.

Zhou, S.-j., H.-h. Zhang, and G.-p. Yang (2018), Distributions and chemical characteristics of water soluble ions in PM2.5 and PM10 over the East China Sea, *China Environmental Science*, *38*(3), 900-909, doi:10.19674/j.cnki.issn1000-6923.2018.0104. *In Chinese.*

Zhou, S., Y. Chen, A. Paytan, H. Li, F. Wang, Y. Zhu, T. Yang, Y. Zhang, and R. Zhang (2021), Non‐Marine Sources Contribute to Aerosol Methanesulfonate Over Coastal Seas, *Journal of Geophysical Research: Atmospheres*, *126*(21), e2021JD034960, doi:10.1029/2021jd034960.

Zhu, C., K. Kawamura, and B. Kunwar (2015), Organic tracers of primary biological aerosol particles at subtropical Okinawa Island in the western North Pacific Rim, *Journal of Geophysical Research: Atmospheres*, *120*(11), 5504-5523, doi:10.1002/2015jd023611.

Variation of the Air Mass Exposure to Chlorophyll Over Eastern China Seas: an Insight into Marine Biogenic Aerosols

Shengqian Zhou[1], Ying Chen[1,2*], Fanghui Wang[1], Yang Bao[1], Xiping Ding[3]，Zongjun Xu[1]

[1]Shanghai Key Laboratory of Atmospheric Particle Pollution Prevention, Department of Environmental Science & Engineering, Institute of Atmospheric Sciences, Fudan University, Shanghai 200438, China.

[2]Institute of Eco-Chongming (IEC), Shanghai 202162, China.

[3]Pudong New District Environmental Monitoring Station, Shanghai 200135, China.

Corresponding author: Ying Chen (yingchen@fudan.edu.cn)

Contents of this file

Additional Supporting Information (Files uploaded separately)

Introduction

This file contains 2 supplementary texts showing detailed information about (1) the field campaigns and chemical analyses, and (2) the data match-up between AEC and marine biogenic MSA for constructing the parameterization scheme. It also contains 10 graphs supporting the methods and main text, as well as the caption for a supplementary table listing historical MSA measurements and relevant information.

Text S1. Cruise campaigns, aerosol sampling, and chemical analyses

We have conducted four seasonal cruise campaigns in the eastern China seas during (1) 27 March to 14 April 2017 (spring), (2) 27 June to 19 July 2018 (summer), (3) 28 December 2019 to 17 January 2020 (winter), and (4) 12 to 29 October 2020 (autumn). Two other cruises in the eastern China seas to WNPO were conducted during (5) 17 March to 23 April 2014 and (6) 30 March to 4 May 2015. The tracks of cruise 1-4 are shown in Figure S2, and the tracks of cruise 5 and 6 can be found in Fu et al. (2018) and Yang et al. (2020) respectively. During the cruises, TSP samples were collected on cellulous filters (Whatman Grade 41) by high-volume samplers with a flow rate of 1.05 m^3 min^{-1}. The duration of each sample was typically 12–24 hours, and the sampling was paused if there was a forward apparent wind or the ship was stopped in order to avoid the exhaust contamination. In each campaign, 2–3 operational blanks were set.

1/32 of each sampling filter was cut and extracted ultrasonically by 20 mL of ultrapure water (> 18.25 MΩ cm^{-1}). The extracting solution was filtered by a polytetrafluoroethylene (PTFE) syringe filter (pore size = 0.45 μm). Then, the concentrations of Na^+, MSA, and SO_4^{2-} were determined by ion chromatography (Thermo, DIONEX ICS-3000). Blank corrections were conducted for all chemical measurements. The ambient mass concentration of nss-SO_4^{2-} was calculated by subtracting sea-salt SO_4^{2-} based on the typical Na^+-to-SO_4^{2-} ratio in seawater: nss-SO_4^{2-} = SO_4^{2-} − 0.251 × Na^+ (Pilson, 2012).
1/16 of each sampling filter was cut was digested with 8 mL of ultrapure HNO_3 and 0.6 mL of ultrapure HF in a microwave digestion system (MARS XPress, CEM). The digested solution was heated and evaporated to about 0.5 mL and then diluted to 15 mL with 2% HNO_3. Then the concentrations of Al and Cd were determined by an inductively coupled plasma mass spectrometry (ICP-MS, NexION 300X, PerkinElmer).

Text S2. Match-up between AEC and marine biogenic MSA

We integrated previously reported MSA measurements and our observations over the eastern China seas (Table S1) and obtained the relationships between MSA concentration and the AEC for each region. As for the 6 cruises we performed (four cruises in the YS and ECS and two cruises in ECS and NWPO), the R_L, AEC, and R_{MBL} for a specific TSP sample were obtained by averaging their values calculated from all trajectories of the sample (trajectory numbers = sampling hours). For autumn and winter cruises, only samples with $R_L < 0.1$ were retained in order to eliminate the impact of terrestrial MSA. For spring and summer cruises, no R_L filtration was applied. Then, the samples with mean $R_{MBL} > 0.9$ were retained and those located in the same region during each cruise were binned. As for other cruise observations collected from previous studies, they were all performed in spring and summer. Because no detailed information about the cruise track history and sampling periods is available, for each cruise, we applied the average AEC value (under the condition of $R_{MBL} > 0.9$) for all 1° × 1° grid cells that ship navigated in a certain region to match the average MSA concentration of all samples. For island-based observations, the AEC (under the condition of $R_{MBL} > 0.9$) in each spring and summer campaign over Huaniao Island and in each month during March to October over Okinawa Island (Zhu et al., 2015) were matched to corresponding average MSA

concentrations. The selection of these campaigns also aims to avoid the significant interference of terrestrial transport.
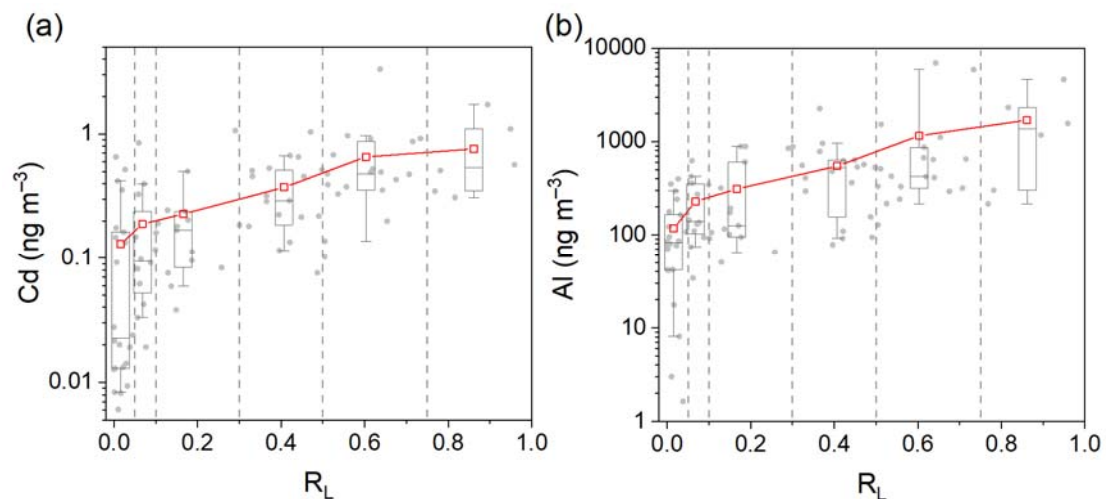
Figure S1. Relationships between (a) Cd and (b) Al concentrations and R_L in four cruises over the eastern China seas during 2017 to 2020. The gray dots represent initial data pairs and the box-whisker plots represent the binned results with R_L boundaries of 0.05, 0.1, 0.3, 0.5, and 0.75, and are drawn for 10-, 25-, 50-, 75-, and 90-percentiles. The red rectangles represent the mean values of each bin.
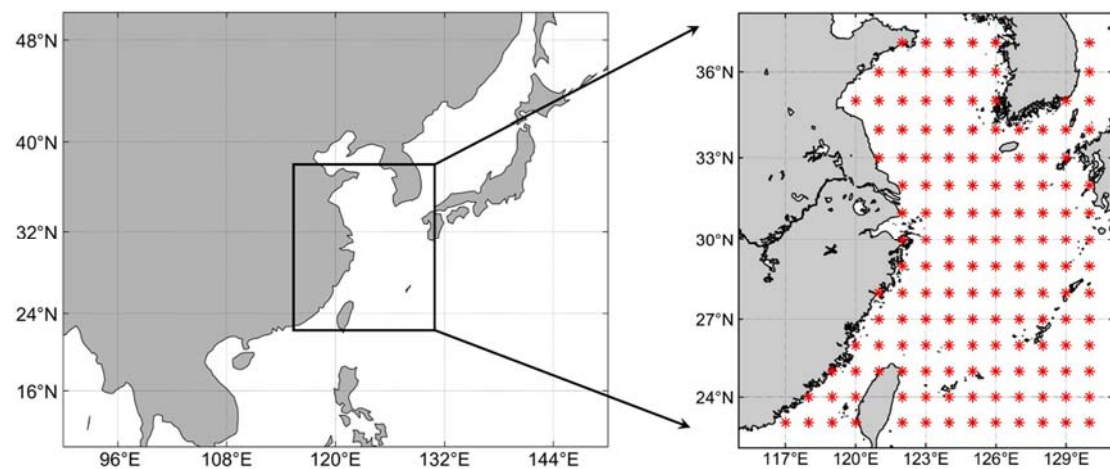

Figure S2. The location of the research region. The red star represents the center of each grid.
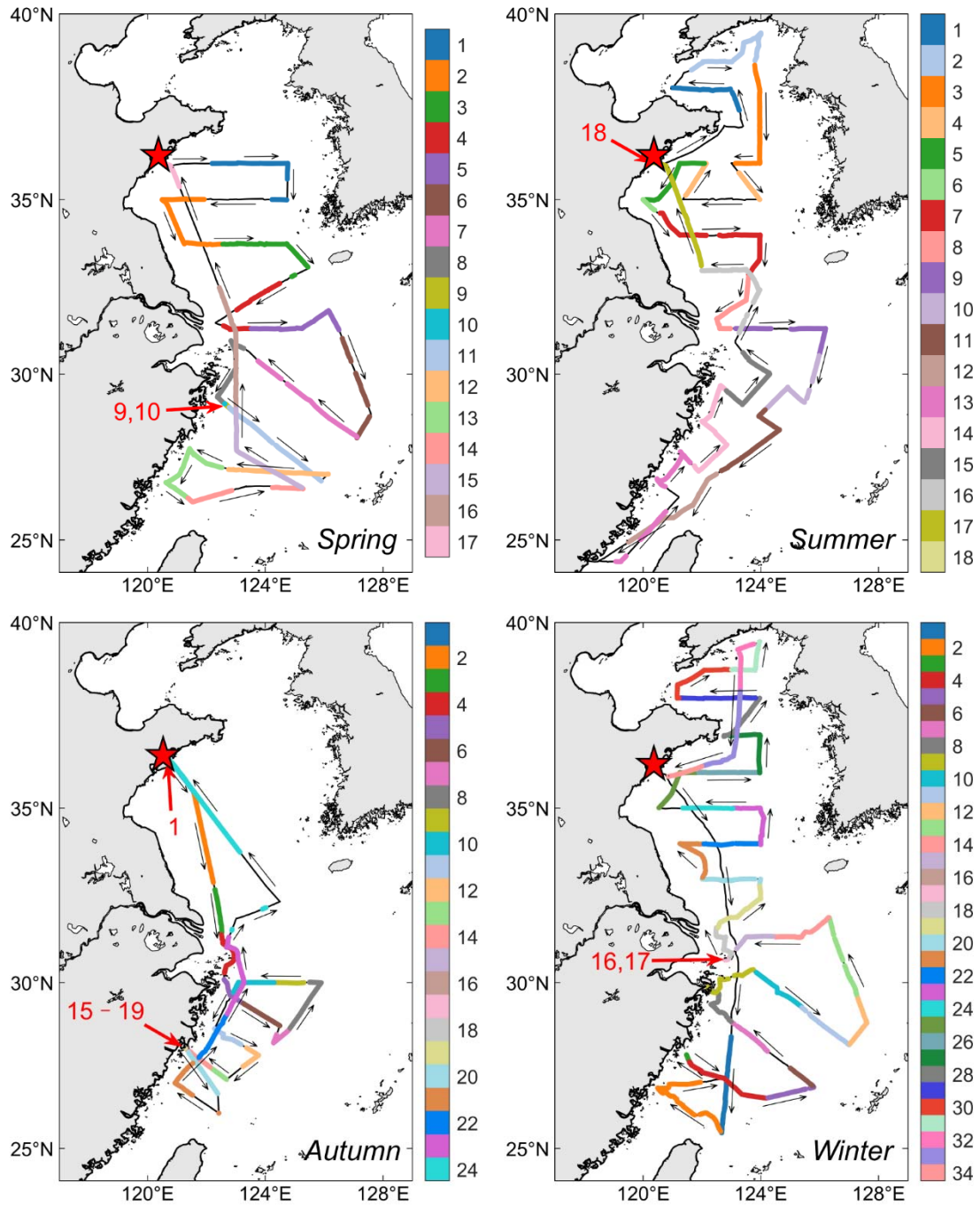
Figure S3. The tracks of cruise 1–4 in the eastern China seas. The cruise segments with different colors correspond to different samples, and the sample IDs are listed as legends. The red star represents the home port of research vessels.
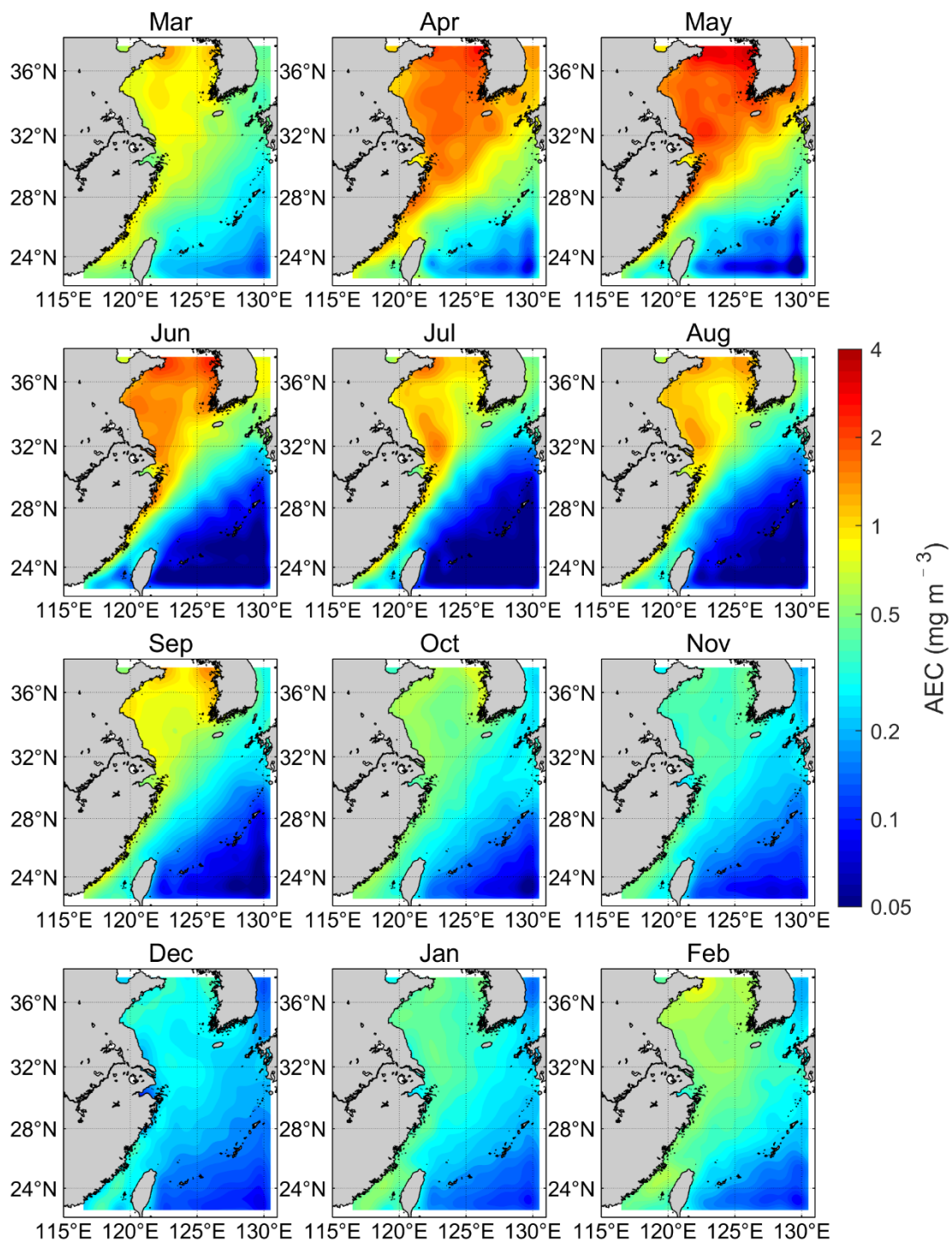
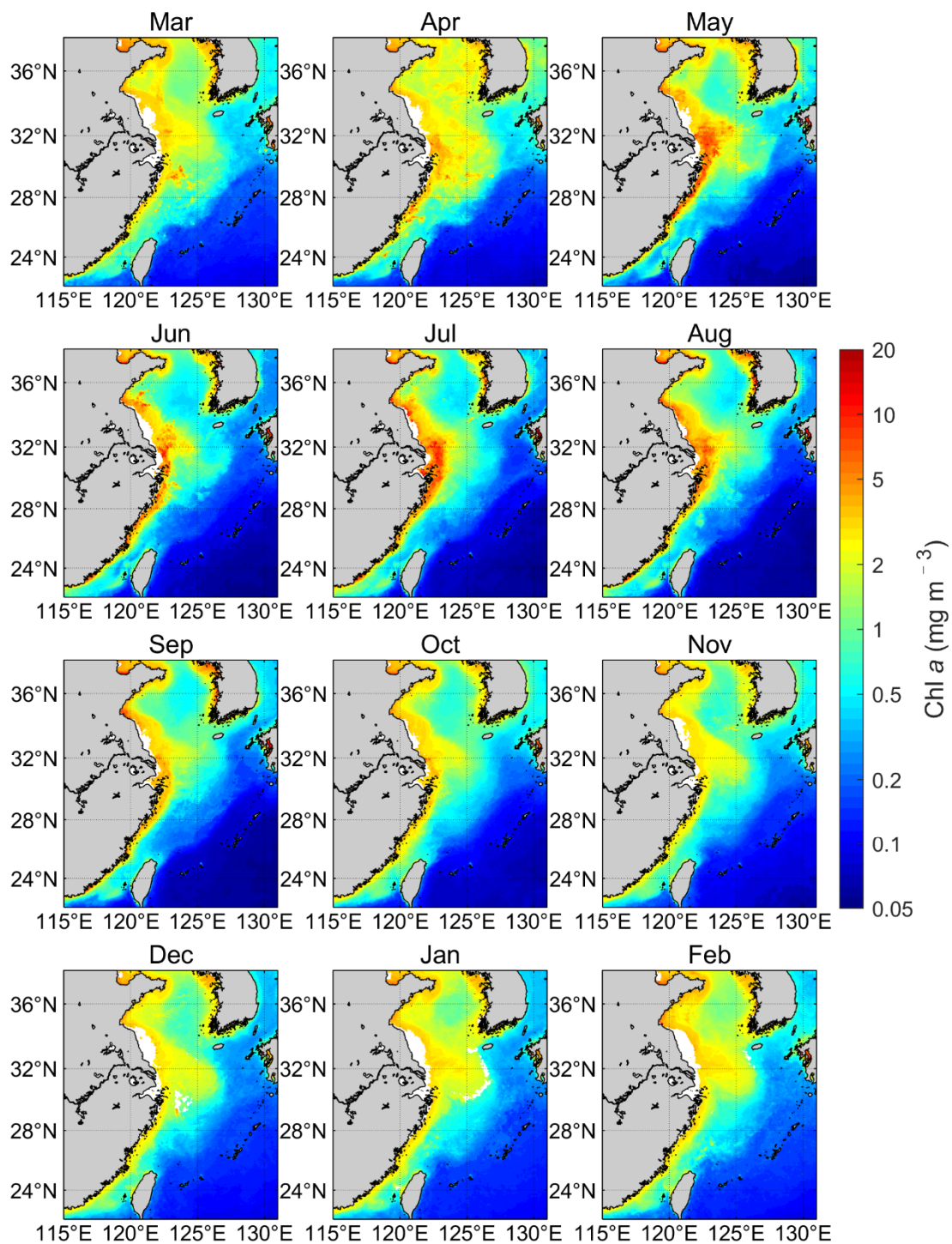**Figure S4.** Monthly climatology for AEC under the condition of $R_{MBL} > 0.9$ during 2009 to 2020.

Figure S5. Monthly climatology for the concentration of sea surface Chl *a* during 2009 to 2020.
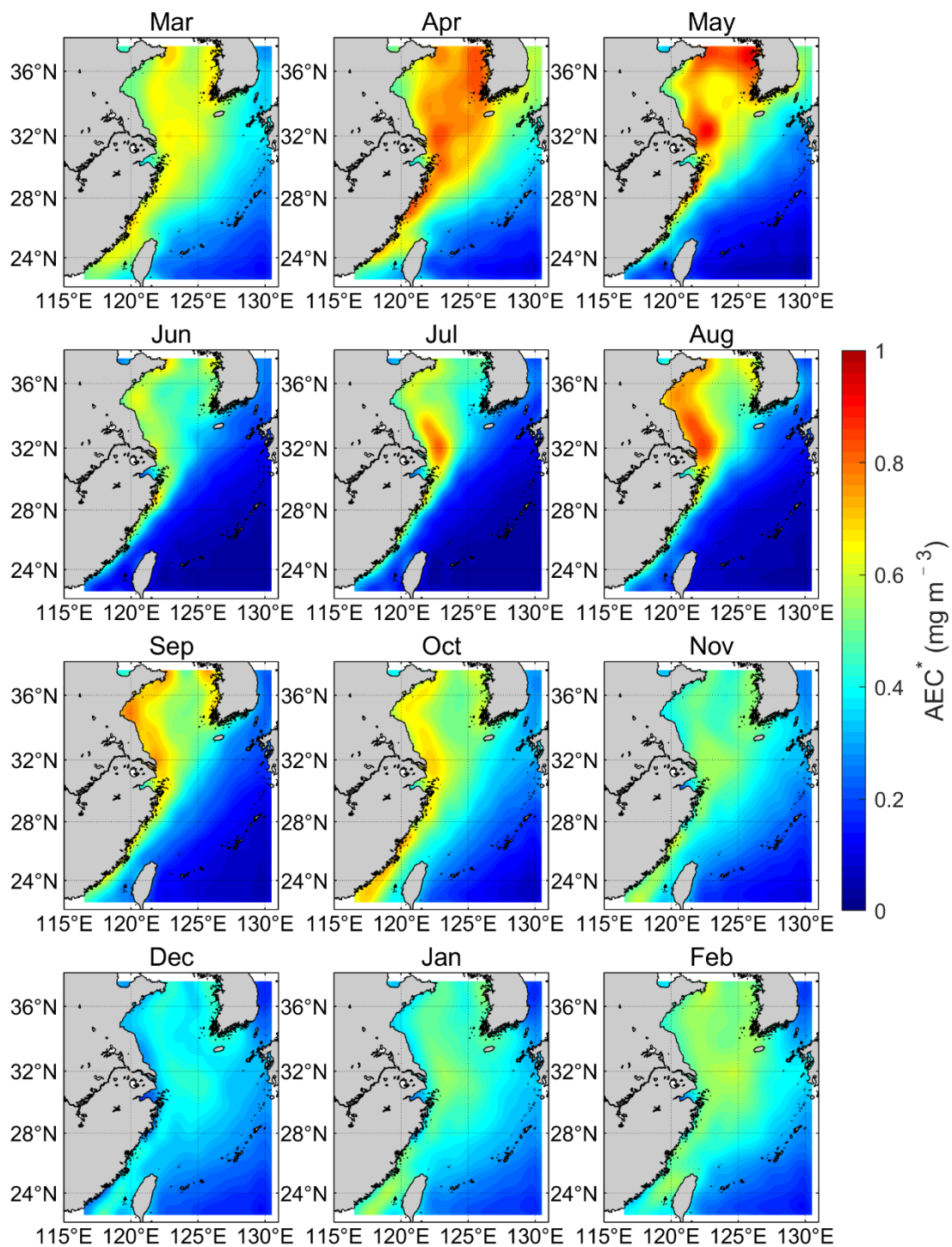
Figure S6. Monthly climatology for AEC index without considering BLH (AEC*) under the condition of $R_{MBL} > 0.9$ during 2009 to 2020.
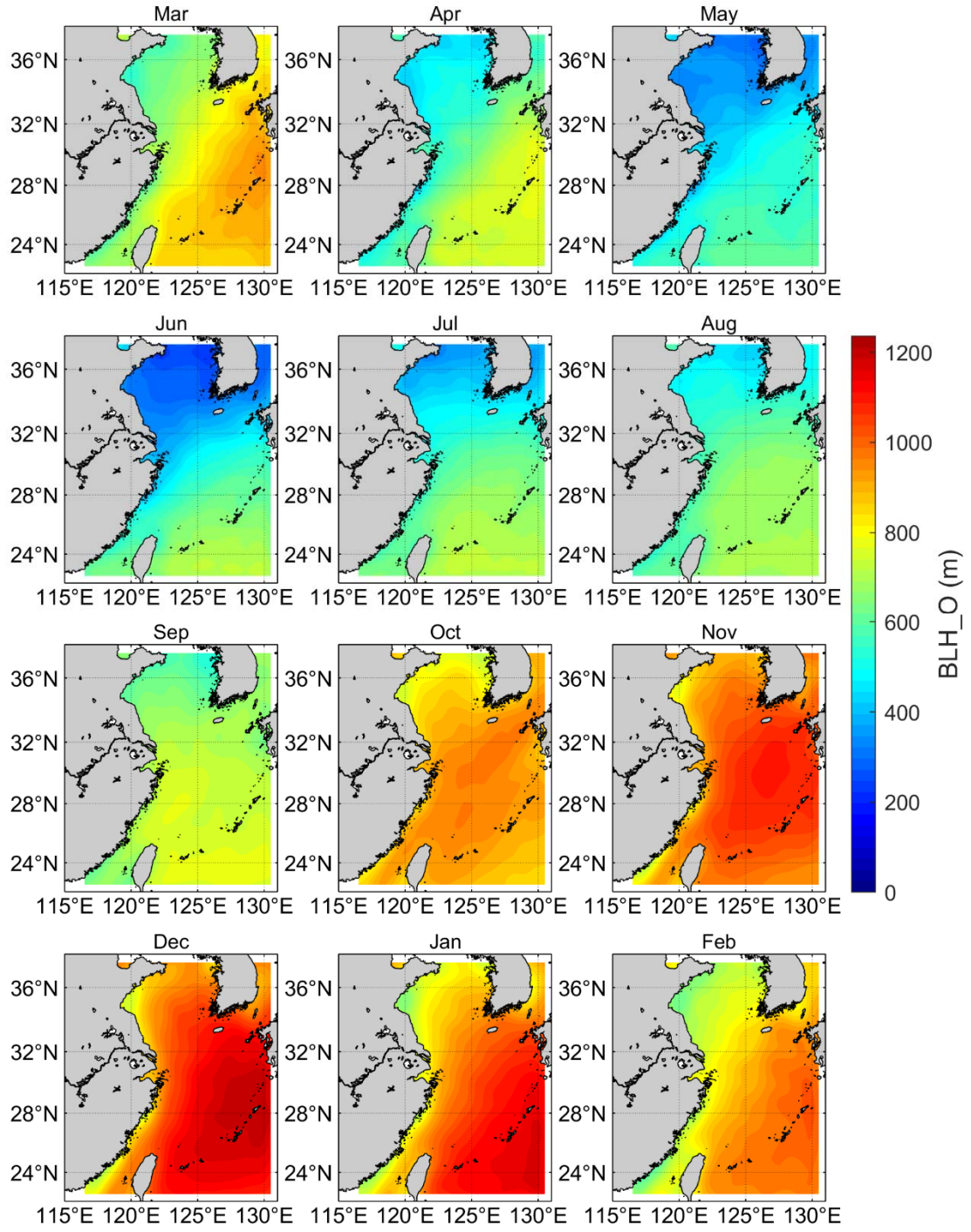
Figure S7. Monthly climatology for BLH along marine trajectory (BLH_O) under the condition of $R_{MBL} > 0.9$ during 2009 to 2020.
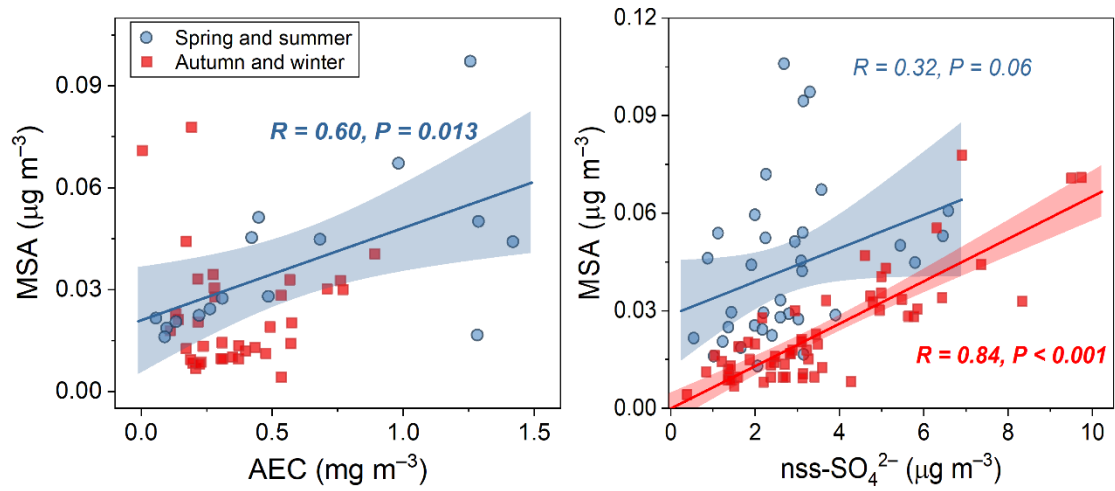
Figure S8. The correlations between MSA concentration and AEC when marine air masses are transported mostly within boundary layer ($R_{MBL} > 0.9$) and between MSA and nss-SO_4^{2-} concentrations in four cruises over the eastern China seas. The blue markers represent data in the spring and summer, while the red markers represent autumn and winter. The thick lines and shaded bands show the linear regressions and their 95% confidence intervals.

Figure S9. Comparisons between MSA/nss-SO_4^{2-} in different R_L ranges for (a) spring and summer cruises and (b) autumn and winter cruises. The box-whisker plots represent the data distributions with $R_L \leqslant 0.2$ and $R_L > 0.2$, and are drawn for 10-, 25-, 50-, 75-, and 90-percentiles. The red rectangles represent the mean values of each R_L range. The P value of the unpaired two-tailed Student's t-test is given.

Figure S10. The average AEC for each region in different months. The shaded band denotes the mean ± SD.

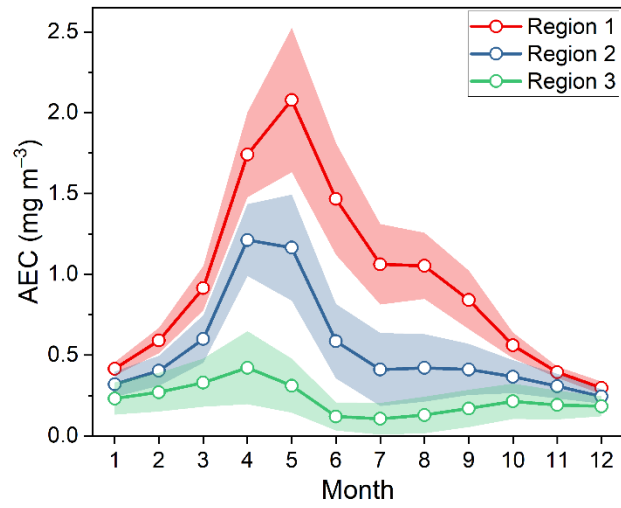**Table S1.** The information about historical MSA observations used in this study.

Table S1. The information about historical MSA observations used in this study.

Region	Latitude (°)	Longitude (°)	Time period	Number of samples	Average AEC (mg m^{-3})	Average [MSA] (μg m^{-3})	Reference
1	26 – 35	121 – 124	31 Aug. – 19 Sep. 2014	14	0.97	0.021	(Ji et al., 2016)
1	33 – 37	120 – 124	21 Apr. – 30 Apr. 2010	7	0.72	0.056	(Xue, 2012)
1	34 – 36	120 – 124	9 Spt. – 14 Sep. 2010	5	0.71	0.030	(Xue, 2012)
1	33 – 36	123 – 125	17 Mar. – 20 Mar. 2011	2	1.60	0.056	(Xue, 2012)
1	33 – 37	120 – 124	27 Apr. – 3 May 2009	5	1.56	0.078	(He, 2011)
1	31 – 36	120 – 122	2 Jul. – 19 Jul. 2018	4	0.93	0.060	This study
1	31 – 36	120 – 133	17 Mar. – 20 Mar. 2014	3	2.11	0.078	This study
1	31	123	22 Mar. – 19 Apr. 2013	10	1.10	0.042	(Zhou et al., 2021)
1	31	123	18 Jul. – 10 Aug. 2013	20	1.56	0.038	(Zhou et al., 2021)
1	31	123	7 Apr. – 2 May 2015	6	1.14	0.057	(Zhou et al., 2021)
1	31	123	4 Aug. – 23 Aug. 2015	12	1.47	0.052	(Zhou et al., 2021)
1	31	123	22 Jul. – 17 Aug. 2016	24	1.39	0.040	(Zhou et al., 2021)
1	31	123	14 Mar. – 17 Mar. 2017	2	0.56	0.016	(Zhou et al., 2021)
1	31	123	1 Jul. – 9 Jul., 28 Aug. – 12 Sep. 2017	18	1.09	0.031	(Zhou et al., 2021)
1	31	123	3 Apr. – 30 Apr. 2018	9	1.02	0.037	(Zhou et al., 2021)
2	28 – 37	122 – 127	5 Jul. – 26 Jul. 2011	9	0.39	0.049	(Zhang et al., 2014)
2	27 – 32	122 – 127	20 Mar. – 30 Mar. 2011	4	0.96	0.083	(Xue, 2012)
2	26 – 32	122 – 125	10 Jun. – 19 Jun. 2010	8	0.29	0.044	(Xue, 2012)
2	25 – 33	121 – 128	4 May – 14 May 2009	8	0.79	0.060	(He, 2011)
2	26 – 30	121 – 125	28 May – 10 Jun. 2014	13	0.40	0.033	(Zhou et al., 2018)
2	27 – 31	123 – 127	2 Apr. – 9 Apr. 2017	5	0.61	0.041	This study
2	24 – 31	120 – 124	6 Jul. – 16 Jul. 2018	6	0.35	0.020	This study

2	26 – 32	122 – 128	28 Dec. 2019 – 7 Jan. 2020	7	0.36	0.028	This study
2	26 – 31	121 – 123	25 Oct. – 27 Oct. 2020	3	0.44	0.020	This study
2	28 – 30	124 – 125	1 Apr. – 2 Apr. 2015	1	1.16	0.076	This study
3	27	128	Mar. 2010	4	0.12	0.040	(Zhu et al., 2015)
3	27	128	Apr. 2010	4	0.20	0.045	(Zhu et al., 2015)
3	27	128	May 2010	5	0.19	0.045	(Zhu et al., 2015)
3	27	128	Jun. 2010	4	0.041	0.028	(Zhu et al., 2015)
3	27	128	Jul. 2010	4	0.034	0.015	(Zhu et al., 2015)
3	27	128	Aug. 2010	4	0.052	0.014	(Zhu et al., 2015)
3	27	128	Sep. 2010	4	0.056	0.016	(Zhu et al., 2015)
3	27	128	Mar. 2011	3	0.40	0.044	(Zhu et al., 2015)
3	27	128	Apr. 2011	4	0.40	0.075	(Zhu et al., 2015)
3	27	128	May 2011	2	0.19	0.019	(Zhu et al., 2015)
3	27	128	Jun. 2011	2	0.039	0.012	(Zhu et al., 2015)
3	27	128	Jul. 2011	4	0.056	0.025	(Zhu et al., 2015)
3	27	128	Aug. 2011	4	0.064	0.071	(Zhu et al., 2015)
3	27	128	Sep. 2011	4	0.17	0.043	(Zhu et al., 2015)
3	28 – 37	135 – 150	22 Mar. – 19 Apr. 2014	13	0.17	0.019	This study
3	25 – 38	124 – 152	4 Apr. – 29 Apr. 2015	16	0.19	0.035	This study